2017

From Dose to Response: In Vivo Nanoparticle Processing and Potential Toxicity

Uschi M. Graham
University of Kentucky, uschi.graham@uky.edu

Gary Jacobs
University of Kentucky, gary.jacobs@uky.edu

Robert A. Yokel
University of Kentucky, ryokel@email.uky.edu

Burtron H. Davis
University of Kentucky

See next page for additional authors

HHS Public Access

Author manuscript

Adv Exp Med Biol. Author manuscript; available in PMC 2019 February 15.

Published in final edited form as:

Adv Exp Med Biol. 2017 ; 947: 71–100. doi:10.1007/978-3-319-47754-1_4.

From Dose to Response: In Vivo Nanoparticle Processing and Potential Toxicity

Uschi M. Graham,
University of Kentucky, Lexington, KY, USA

CDC/NIOSH DART, Cincinnati, OH, USA

Gary Jacobs,
University of Kentucky, Lexington, KY, USA

Robert A. Yokel,
University of Kentucky, Lexington, KY, USA

Burtron H. Davis,
University of Kentucky, Lexington, KY, USA

Alan K. Dozier,
CDC/NIOSH DART, Cincinnati, OH, USA

M. Eileen Birch,
CDC/NIOSH DART, Cincinnati, OH, USA

Michael T. Tseng,
University of Louisville, Louisville, KY, USA

Günter Oberdörster,
University of Rochester, Rochester, NY, USA

Alison Elder, and
University of Rochester, Rochester, NY, USA

Lisa DeLouise
University of Rochester, Rochester, NY, USA

Abstract

Adverse human health impacts due to occupational and environmental exposures to manufactured nanoparticles are of concern and pose a potential threat to the continued industrial use and integration of nanomaterials into commercial products. This chapter addresses the inter-relationship between dose and response and will elucidate on how the dynamic chemical and physical transformation and breakdown of the nanoparticles at the cellular and subcellular levels can lead to the *in vivo* formation of new reaction products. The dose-response relationship is complicated by the continuous physicochemical transformations in the nanoparticles induced by the dynamics of the biological system, where dose, bio-processing, and response are related in a

Correspondence to: Uschi M. Graham.

non-linear manner. Nanoscale alterations are monitored using high-resolution imaging combined with in situ elemental analysis and emphasis is placed on the importance of the precision of characterization. The result is an in-depth understanding of the starting particles, the particle transformation in a biological environment, and the physiological response.

Keywords

Nanotechnology; Electron Microscopy; Transformation; Subcellular; Nanoparticle Instability

4.1 Introduction

Nanotechnology is a key modernization driver that balances innovations in material synthesis with the need for novel solutions that impact all energy sectors, emerging medical fields, and rapidly evolving electronics applications [3]. It also offers environmental technology breakthroughs by integrating nanotechnology products and synthetic biology and offers opportunities that focus on human health and animal welfare. The field of nanomaterials is a multidisciplinary area in which material science is explored at the nano-scale, but the concepts behind nanoscience are not new. In his celebrated lecture at Caltech, in 1959, physicist Richard Feynman described the process of manipulating and controlling individual atoms, molecules and nanoparticles, and he anticipated an “enormous number of technical applications” through the creation of novel materials and compounds [22, 76, 78]. More than half a century later, scientists and engineers are finding various ways to produce a wide range of nanoparticles [1]. Importantly, the fast exploration and deployment of nanomaterials must also incorporate exposure, toxicity and risk assessment studies in order to balance the successful integration of nanomaterials into everyday life with any potential safety and environmental issues [7, 17, 18, 48, 58, 69, 72, 78]. This is critically important in determining which parts of life may be enriched with the assistance of nanomaterials and which parts may suffer.

Manufactured nanoparticles (MNPs) typically range in size from 1–100 nm [23]. They exhibit unique properties compared with those of their larger-sized “macro” counterparts. The differences are due to vastly increased surface-to-bulk ratios and because of the distinct structures of MNPs [13, 27, 80, 88]. Nanotechnology and the application of nanoparticles in consumer products has become an integral part of today’s life and require safety assessments [4, 12, 20, 27, 32, 34, 50, 59, 66, 73]. The growing rate of nanoparticle-based product developments has raised worldwide apprehension regarding the release of MNPs into the environment and their subsequent uptake. There are several uptake pathways for MNPs, which complicates the issue of modelling exposure risks tremendously [5, 15, 30, 40, 54, 60, 83]. Nano-safety studies have seen an exponential rise over the past two decades, but the effects and dangers of nanoparticles, either for animals, humans, or cell structures, are still not clearly defined [10, 43]. Safety concerns have led industrial and academic researchers to adopt strategies to make MNPs more biocompatible, by employing techniques such as capping with various functional groups and also by exploring new synthesis routes [64], but the ultimate fate of the MNPs after uptake remains unresolved [28, 56, 85]. This is, in part, heightened by additional effects from nanoparticles that come from sources other than

controlled manufacturing labs, such as pollution-derived nanoparticles where the composition, size ranges and effects are often unknown. Another important issue is the environmental significance of natural colloids and nanoparticles that govern elemental mobility and bio-availability [33], where much of the environmental pool of nanoparticles consists of breakdown products from both organic and inorganic sources such as cellulose fragments and clays that may be in the same size range as MNPs. There is also the influx of pollution-derived nanoparticles produced in urban settings from industrial effluents and auto exhausts, which are an important part of risk assessment models and have been linked to major health problems [11, 19, 88].

Adverse human health effects due to occupational and also environmental exposures to nanoparticles are of worldwide concern. Concepts of nanoparticle dose metric and response metric are of paramount importance [42, 43] and can provide key insights into relationships between the nanoparticles' synthetic identity and chemical reactivity, their biological activity which involves aggregation, protein interactions, protective surface coatings as well as migration and, lastly, their stability, all of which contribute individually and collectively to dose-dependent toxicity outcomes [79]. An in-depth understanding of biokinetics is vital to obtaining meaningful risk assessment protocols for MNPs [71, 78, 87]. This has to include information on the biodistribution and clearance of MNPs as a function of the exposure route [43]. Furthermore, it has to include information on uptake, transport and transformation of MNPs as a function of dose and epithelial route of entry (including but not limited to gastro-intestinal, dermal and respiratory ports-of-entry). It also requires thorough data collection on the biotransformation of MNPs within target tissues and cells [27]. The cellular and subcellular interactions of nanoparticles are a function of the physiological environment which can only respond to a certain number of invader nanoparticles or reactive surface area (smaller nanoparticles contribute higher surface areas and in this regard, also contribute different surface properties such as charge, composition, structures, porosity, redox-state and reactivity). This is sometimes referred to as the "surface area dose-response relationship" [61] and affects the short and long term fate of nanoparticles after uptake. Dose and nanoparticle properties (nano-design) will undoubtedly influence the transport and bioprocessing (*in vivo* effect) of the MNPs and their derivatives (break-down products) which leads to a dose-dependent reactivity and physiological response (nanotoxicity) (Fig. 4.1).

A dose-dependent instability of synthesized MNPs after exposure and cellular uptake leads to *in vivo* processing and transformation, which may be followed by a certain response (oxidative stress and inflammation) and ultimately results in nanotoxicity (Fig. 4.1). Clearly, a nanoscale substance might potentially be toxic for a biological system when the "dose" or concentration exceeds an adverse threshold. The response "effect" could be initiated by a single "acute" dose, or, by repeated low "chronic" dose that occurs over an extended time frame. Careful dose evaluations are necessary for meaningful risk assessments of nanoparticles and play a major role in regulatory processes to help determine health-relevant limits [43]. For example, instillation studies are typically carried out with high MNPs doses and it is impossible to know whether effects are caused by overload conditions or due to the MNPs' inherent effects. Inhalation studies can offer insights at lower dose, yet they too are met with inflammatory responses which have been determined more often than not to be

independent of the nature of MNPs that are inhaled [43, 88]. Because of these difficulties in dose-response studies, the mechanisms that induce toxicity from respiratory exposures are poorly understood and thus hinder the building of predictive models. Similarly, low dose response studies for MNP exposures to skin and gastrointestinal epithelial tissues are lacking as is our understanding of how differences in the local biological milieu effects microenvironment around a nanoparticle and vice-versa.

4.1.1 In Vivo Processing and Transformation of Nanoparticles

The issue that will be addressed in this chapter is the relationship between dose and potential *in vivo* processing of nanoparticles (response) shown in Fig. 4.1. The issue includes nanoparticle uptake, transport and transformation as a function of dose and uptake routes. *In vivo* processing is defined here as the dynamic chemical and/or physical breakdown of nanoparticles at the cellular and subcellular level [27]. The process can be followed *by in vivo* formation of new reaction products including ions, nuclei and growth of second generation nanoparticles all of which may be set in motion by the breakdown of the original nanomaterials. Such *in vivo* biotransformation processes are known to occur with implanted orthopedic materials that can lead to both pathologic and beneficial patient outcomes. For example, nanoparticle wear debris formed from articulating prosthetic surfaces can lead to osteolysis [29], whereas the successful adherence and osteoinduction of amorphous bioactive glass results from a dissolution and re-precipitation reaction and induces a material phase change to crystalline hydroxyapatite [35, 39].

Uptake and transport of nanoparticles to different regions in the body have been extensively studied and are generally linked to certain pathology and toxicity [40, 43, 51, 52, 56, 61]. However, the *in vivo* breakdown and processing of MNPs that leads to formation of new reaction products with different properties is not very clear and obfuscates the issue of exposure risk and related outcomes. It also makes the design of meaningful predictive models significantly more challenging. The breakdown mechanism of MNPs in cells depends on the material composition, surface coatings, ports of entry and the organs they invade (Fig. 4.2). The instability of nanoparticles in cells then initiates another cascade of responses that yet have to be defined. In this Chapter, we describe applications of advanced electron microscopy methods to the analysis of fixed tissue sections, which provides critical information on material phase changes and the oxidation states of MNPs [27]. Specifically, we discuss use of high resolution (nanometer) transmission electron microscopy (HRTEM) coupled with simultaneous elemental analysis for the investigation of the *in vivo* processing of nanoparticles as a function of dose and uptake route (Fig. 4.2). The *in vivo* processing evidence can then be used for more comprehensive modelling of the potential exposure risks for nanoparticles. The goal of these studies is to investigate cellular and subcellular interactions of MNPs using advanced imaging and analysis of the retained particles and correlate these interactions with biological and toxicological effects. The data are important to build meaningful predictive models that are based on the dynamic interaction of nanoparticles at the cellular and subcellular levels after uptake. A thorough understanding of nanoparticle processing in biological systems as a function of dose is vital in making determinations of the long-term toxicological effects. This requires studies to determine *in vivo* solubility (nanoparticle dissolution), size and shape changes in response to the original

dose and nanoparticle retention time (Fig. 4.2). A possible increase or decrease in protein corona around the MNPs and their cell associations also must be examined [14, 25]. *In vivo* processing of MNPs is a function of dose and residence time in particular tissues or cells. The *in vivo* processed nanoparticles and any "newly" formed phases and reaction products must be compared with the original MNPs (Fig. 4.2). The nanoparticle's characteristic "fingerprints" before and after *in vivo* processing are based on composition, geo metrical parameters and physiochemical, structural and spectroscopic properties. Without this data, it would be impossible to build meaningful models that correlate nanoparticle dose and exposure risks. However, a deep understanding of biokinetics is also central to obtain an all-encompassing exposure risk assessment and involves identification of target organs following different routes of exposure. One has to evaluate the *in vivo* processing of MNPs not only in the regions where uptake first occurs (portal-of-entry-organs), but also must observe any particle breakdown or processing in secondary and further ancillary target tissues while considering the original dose and residence time of the particles. Often the experimental characterization of nanoparticles that is obtained before exposure is directly linked to cellular-based assays. This means that risk assessment models typically assume that the "invader" nanoparticles that cause toxicity are exactly the same as those that were used in the exposure experiments. Unfortunately that is an oversimplification. To date we know that nanoparticles are processed *in vivo* [28] and the extent to which they are processed needs to be systematically studied so that this information can be incorporated into advanced risk assessment models. Future studies will need to evaluate the *in vivo* processing of MNPs in portal-of entry organs and also in secondary target tissues and evaluate any modifications/transformations of MPNs with regards to their physicochemical changes as a function of the route and duration of exposure. Only then can predictive models be designed to better forecast nanoparticle-dose-toxicity relationships. State of the art microscopy methods can be applied to obtain needed *in vivo* processing data, and several examples of this approach are presented in the remainder of this Chapter.

4.2 The Role of Cellular Breakdown and In Vivo Processing of Nanoparticles

The study of *in vivo* induced changes to nanoparticles is an emerging area of investigation. In the case of highly soluble materials such as nano-copper and nano-silver any dissolution and particle breakdown after uptake into biological media can be expected and has been demonstrated [6]. However, the *in vivo* breakdown and transformation mechanisms of essentially poorly soluble particles (PSP) like ceria (CeO_2) on a cellular and subcellular level are not well understood. The breakdown mechanism of CeO_2 nanoparticles in the liver of rats was recently demonstrated for the first time [27]. These findings confirm that nanoparticle uptake and sequestration in peripheral organs can lead to the formation of secondary particles with different physiochemical properties including altered reactivity and effects that result in varying degrees of toxic effects over long periods of exposure. Furthermore, ceria *in vivo* transformation can progress to a toxic, more benign, or potentially beneficial state [32]. In this regard, CeO_2 nanoparticles after prolonged residence time of 90 days inside liver undergo *in vivo* processing that causes a shift towards smaller particle size and an increased reactive surface area with enhanced free radical scavenging

potential of the new *in vivo* formed ultrafine particles [27]. This work also showed with the help of high resolution imaging and analysis that essentially insoluble CeO_2 nanoparticles experience partial dissolution and reformation inside the liver. Breakdown and redistribution after inhalation of ceria nanoparticles could be a possible coping mechanism of biological systems and a step towards improving nanoparticle biocompatibility as illustrated in Fig. 4.3.

Because CeO_2 is basically insoluble under laboratory controlled conditions, one has to question what drives dissolution of CeO_2 and similar nanoparticles in the liver, lung and possibly other regions *in vivo* and whether enzyme activity and other factors need to be incorporated into risk assessment models. This is particularly important for more soluble nanoparticles such as amorphous silica (SiO_2), alumina (Al_2O_3), titania (TiO_2) and iron oxides (Fe_2O_3 and Fe_3O_4) which constitute the vast volumes of MNPs used today in consumer products and medical imaging. Faster dissolution rates could lead to rapid particle breakdown and transformation. Clearly, how to obtain insights into biotransformation routes of nanoparticles and their *in vivo* processing response depends on well-designed experimental studies that provide dose-controlled nanoparticle uptake, i.e., via instillation, inhalation (lung, olfactory system), oral intake (stomach, GI) or dermal uptake (skin: intact versus injured) (Fig. 4.2). This has to be followed by a systematic comparison of the *in vivo* transformed particles with the pristine precursor materials by examining morphological changes, size variations, dissolution patterns and the presence or absence of secondary reaction zones (new precipitates) in the vicinity of the transforming nanoparticles. Further detailing the physio-chemical changes during bioprocessing of nanoparticles may be an effective tool in understanding their subcellular and temporal fate that controls toxicity. These analyses depend on advanced imaging methods. High-resolution electron microscopy applications allow the use of fixed tissues to examine nanoparticle location, size and composition immediately after deposition and also after prolonged residence time. Nanoparticle-cell interaction and dose-dependent inflammatory response raises the question about underlying cellular mechanisms that produce nanoparticle instability (Fig. 4.2). Therefore, dose-dependent toxicity that is caused by *in vivo* processing of nanoparticles needs to be considered in risk assessment models. Also, it is important to model nanotoxicity as a function of the nanoparticle instability, transformation, mobility and potential *in vivo* reformation (precipitation) at the cellular and subcellular level. Nanoparticle instability *in vivo* is a function of the particle's inherent composition, size, molecular structure and surface chemistry among other properties, but also a function of the complex cellular condition such as protein corona, inflammatory responses (chronic vs. acute), upregulation of inflammatory defense mechanisms and availability of enzymatic catalysts just to name some. Mobility of individual nanoparticles may be controlled by both physical transport of the intact particles, and also by a sequence of dissolution and reformation steps. High resolution analysis of the reaction zones around dissolving nanoparticles in phagolysosomes show breakdown patterns, void spaces and pore-formation, suggesting that there are continuous processes that release and relocate molecules during the nanoparticle transformation. This information is important in creating government regulations for nanoparticle exposure to workers and consumers. One very important aspect for obtaining nanoscale structural and chemical information to be able to study the breakdown and processing of MNPs, of course, is the preparation and conditioning of tissue

materials which precedes all of the advanced imaging and analysis techniques. We refer here to previous works that give excellent overviews of the tissue preparation techniques [49, 55, 74].

The following sections will discuss the importance and application of advanced imaging methods to help identify the various processes involved during *in vivo* nanoparticle transformation and give three specific examples for: (1) high and low dose inhaled amorphous silica (SiO_2) nanoparticles that are deposited, transformed and relocated inside rat lung; (2) ceria (CeO_2) nanoparticle dispersion and *in vivo* processing in spleen after a single high dose instillation; and (3) discuss the spatial and temporal relationship of *in vivo* synthesized ferritin nanoparticles (iron oxy-hydroxide Fe-OOH) as a direct response to the uptake and processing of invader SiO_2 and CeO_2 nanoparticles, and suggest mechanisms at the cellular and subcellular levels.

4.3 Advanced Imaging and Analysis of Nanoparticles in Tissue Sections

The study of nanoparticle *in vivo* processing is compounded by the number of variables in play when it comes to biotransformation, such as composition, morphology, size, and exposure mechanism or route of entry. The situation is made even more complex for researchers in that specialized methods of investigation are required to observe nanoparticle transformations in biological systems. Typical methods employed in biological research can only partly reveal nanoparticle transformations or information about the mechanisms involved due to the small size range. These methods include fluorescence, confocal, and polarized microscopy, electron micro-graphs, radiological tracing, and measurements of biological toxic response indicators. Traditional material characterization methods used by material engineers/scientists need to be employed that allow resolution and analysis at the nanoscale. Methods that have been employed so far are the standard electron microscopy techniques used in materials characterization such as, electron diffraction [2, 27, 46], and scanning transmission electron microscopy (STEM) [81] with the associated analytical techniques energy dispersion spectroscopy (EDS) [36, 84], and electron energy loss spectroscopy (EELS) [16, 26, 80]. Also, x-ray photoelectron spectroscopy (XPS) has been used [27]. Aberration corrected STEM allows imaging at the atomic scale and will be instrumental in determining the structures and composition of *in vivo* formed nanoparticles that are only a few nanometers or possibly sub-nano size [57]. The use of these methods is complicated by the nanoparticles being hosted inside a biological matrix. This requires modifications to the standard biological sample preparation techniques [49, 55, 74].

4.3.1 High Resolution Analytical Microscopy

Electron microscopy has been fundamental in gaining knowledge about biological systems since the 1950’s and was instrumental in developing insights into cellular ultrastructure [21]. As electron microscopes evolved, the imaging needs of the biologist and that of material scientist diverged. The biologist needed high contrast, wide field, and low accelerating voltages, whereas the material scientist needed high resolution imaging, high accelerating voltages, and high brightness through the use of a field emission electron source. This resulted in differing classes of electron microscopes being manufactured such as the Philips

201 and CM-10 for biological applications versus the Philips 300, 400, and CM-12 for material characterization. This has resulted in major medical research centers having biologically oriented electron microscopes with an inability to apply what are now common material characterization techniques. Multidisciplinary collaborations between medical researchers and material scientists can overcome this. High-resolution transmission electron microscopy (HRTEM), coupled with advanced detectors allows one to probe materials in unprecedented detail, providing both local chemical information and also structural properties.

An analytical electron microscope today can image and obtain compositional and electronic information down to the angstrom level. This ability provides highly local information from surface-environment interactions such as *in vivo* nanoparticles. Other material characterization techniques work for bulk samples and have resolutions larger than several nanometers. Thus, for the study of *in vivo* transformation of nanoparticles there is only one choice, an HRTEM designed for materials analysis [28, 84]. A typical HRTEM used in materials characterization will have both TEM and STEM capability with EDS and EELS being incorporated with the use of computer technology to allow the acquisition of elemental line profiles and maps acquired in STEM mode. This allows not only elemental analysis but also acquisition of material phase changes and oxidative states via the EELS data [16, 53]. Combining these observations with material phase databases such as the Materials Project (www.materialsproject.org) and computation from first principles using spectroscopy oriented software such as FEFF9 [67] in principle, allows the identification of phases and electronic states. Because a standard non-aberration corrected field emission electron microscope designed for materials analysis will typically be able to achieve a STEM spot size of 0.2 nm, changes in nanoparticle surfaces versus their main bodies can be analyzed [27]. This data combined with material phase structure data and spectroscopy computation can, in principle, provide information on structural and electronic changes in nanoparticles in tissue. This is the type of information needed to understand the interaction of a nanoparticle with its local environment in order to gain an understanding of the mechanisms behind *in vivo* transformation and how this relates to toxicity.

4.3.2 Example I: Amorphous Silica (SiO_2) Inside Lung Tissue

Analysis of the clearance kinetics using modelling of retained lung burden of SiO_2-MNPs showed a significant *in vivo* solubility which raises questions about underlying cellular mechanisms that result in the instability of the SiO_2-MNPs and related toxicity [24]. This was the stimulus to use HRTEM applications and to look for evidence of particle breakdown and mobility in the lung tissue at both cellular and subcellular levels. The principal objective for HRTEM is to examine any nano-scale alteration, dissolution and processing of SiO_2-MNPs after inhalation by comparing the translocated particles with the precursor SiO_2-MNPs. A dose and time controlled inhalation study involved groups of rats that were exposed to aerosols containing amorphous SiO_2-MNPs for 4 h/day, 5 days/week for 4 weeks with a 27 day post-exposure observation period at three different concentrations and dose-dependent pulmonary inflammation in the rats, and data was collected in relation to the exposure time and corresponding dose that was used [62]. In this particular study, sub-chronic inhalation exposures of the SiO_2-MNPs were investigated using an approach of

dosimetric modelling to determine the mechanisms for clearance of these nanoparticles from the lung. Both mechanical clearance and partial dissolution have to be considered as potential pathways. Determining the *in vivo* bioprocessing mechanisms of the nanoparticles will be important towards risk characterization and to better assess possible health effects caused by the transformation, translocation and clearance of the particles after exposure. The HRTEM observation of the precursor (as synthesized) SiO_2-MNPs particles showed a typical size of ~20–50 nm with a corresponding spherical morphology of the individual aerosolized SiO_2-MNPs components (Fig. 4.4). Furthermore, after 27 days post-exposure the phagocytosed SiO_2-MNPs that were sequestered in alveolar macrophages in the fixed tissue sections were imaged using high resolution Dark Field STEM. The STEM images show clear indication of significant *in vivo* breakdown and transformation (Fig. 4.5). There is also structural evidence in the Dark Field STEM (Fig. 4.5) that a portion of SiO_2-MNPs had been completely dissolved out. The degree of *in vivo* processing of the particles and partial dissolution most likely depends on the residence time, dose, and synthetic identity of the original inhaled SiO_2-MNPs. Most of the SiO_2-MNPs particles lost their original spherical morphology after prolonged lung retention and are now displaying various dissolution patterns (pitting), void formation and secondary outward growth that results in the formation of multiple reaction zones. To gain greater insights into what controls particle transformation and determine if there are any relationships with subcellular components, one has to perform detailed elemental mapping of the regions of interest. As an example, elemental EDS maps of O, Si, S and P (Fig. 4.6) are obtained from a region that is illustrated in the Dark Field STEM image in Fig. 4.5. The EDS elemental maps of O, Si, S, and P require the use of a 1 nm STEM probe to have enough counting statistics within a reasonable dwell time as illustrated in (Fig. 4.6).

Typically a 1–2 s dwell time is used depending on the signal strength. EELS mapping can be done with a 0.2 nm probe and dwell times as small as 0.1 second, depending on the elemental edge being mapped. Higher edges require longer dwell times. When doing simultaneous EDS and EELS mapping a compromise must be worked out to have a long enough time for a good EDS count and short enough so as not to overload the EELS CCD detector [27]. Other EELS acquisition parameters such as dispersion and y-binning can be adjusted to obtain a satisfactory EELS signal [16, 26]. After performing EDS mapping of a region that seems to have undergone *in vivo* processing of SiO_2-MNPs in alveolar macrophages the O and Si signals clearly follow the outline of the SiO_2-MNPs (Fig. 4.6). However, the Si signal furthermore is indicating that some Si is present in the close neighborhood of the SiO_2-MNPs, while the O signal is predominantly confined to the outline of the alveolar macrophage-entrapped nanoparticles and not seen in the immediate subcellular surroundings. Some O may be present in –(Si-O-Si)- forming anionic silanol components within the tissue and this could be a critical mechanism for Si transport and new precipitates and studies are needed at the molecular level to determine the processes involved in Si mobility after processing of the MNPs. The elemental scans for S and P were included here to show that, surprisingly, the signals are shadowing the location of the SiO_2-MNPs. This opens chief questions for future work including queries into the underlying *in vivo* processing mechanisms that guide nanoparticle delivery to certain cellular and subcellular locations and chemical environments after uptake and also how this may be

affected by dose. The dose variations (high vs. low) all resulted in significant *in vivo* processing of the SiO_2-MNPs after inhalation which probably is based on the relatively high solubility of amorphous silica [9, 24, 31]. Importantly, *in vivo* processing gives rise to second generation nanoparticles and reaction zones containing Si- phase within the vicinity of the bio-transformed SiO_2-MNPs, which suggests that migration and relocation processes take place at the cellular and subcellular levels as determined in elemental mapping (Fig. 4.6). Moreover, high resolution STEM coupled with EDS confirms that release of Si ions and relocation and precipitation of secondary Si- phases in the alveolar macrophages results in generation of Si-rich halos "Si-clouds" at the outskirts of partially dissolving SiO_2-MNPs (Fig. 4.7). An analogous cloud-formation process was shown for the first time to take place when poorly soluble ceria (CeO_2) nanoparticles bio-process in liver tissue [27].

Detailing all of the physio-chemical changes that take place during bioprocessing of SiO_2-MNPs in alveolar macrophages and other tissue locations as a function of dose is still under development. This may be an effective tool in understanding their subcellular and temporal fate and how this factors into controlling a toxic response after environmental uptake of nanoparticles. More work is needed to study the dose effects on the extent of SiO_2-MNPs breakdown and the relocation of Si as a function of saturation levels. An example of further detailing the chemical and structural content of the Si-Cloud contents is shown in the Dark Field STEM images that demonstrate a greater extent of *in vivo* processed SiO_2-MNPs in the alveolar macrophage and the development of nanozone formation (Fig. 4.8). The chemical breakdown of the SiO_2-MNPs (Zone I) leads to pitting in the original particles with subsequent material migration and relocation into satellite zones (Zone II in Fig. 4.8) which hosts much smaller particles that are highly dispersed. This is the reason why Zone II appears less dense and concentrated in the Dark Field STEM image. It will be of paramount importance to apply aberration corrected STEM and 3D– imaging to probe the chemical composition of the matrix of Zone II that engulfs the very small SiO_2-MNPs. If Zone II matrix is chemically distinct from other nanoparticle- free regions in the alveolar macrophage that hosts the SiO_2-MNPs it can help determine if protein formation or encapsulation helps stabilize the SiO_2-MNPs and make them more biocompatible after *in vivo* processing.

The examples above show that *in vivo* processing of nanoparticles can occur and that a materials-oriented electron microscope can reveal some aspects of the changes that are occurring. This coupled with toxicological response monitoring could provide information as to whether nanoparticle dose-dependent changes reduce or increase toxic effects. Much work remains to be done in determining the *in vivo* properties of the many different types of nanoparticles and how variables such as particle morphology, size, surface treatments, and composition effect *in vivo* processing. The application of aberration corrected electron microscopes to the study of *in vivo* processing would most likely be very fruitful [65, 86]. These microscopes have the resolution to determine if a cloud surrounding a nanoparticle is composed of single molecules or very small clusters as in the silica examples above. It could also determine if the composition of such clusters is that of the precursor particle or if a reaction has occurred thereby modifying the clusters and resulted in new compounds. In addition aberration-corrected STEM could provide high resolution maps of the surface layers of nanoparticles and corresponding surrounding tissue to better understand the

mechanisms behind *in vivo* processing. Importantly, aberration-corrected electron optical sectioning can give insights into any potential protein corona formation at the exterior of the nanoparticles. Recently, RAMAN mapping has also become commercially available. This opens the possibility of identifying molecular changes in the tissue surrounding nanoparticles *in vivo* as a function of dose.

4.3.3 Example II: Ceria (CeO_2) Nanoparticles Inside Spleen Tissue

EELS analysis was performed on a 200 kV JEOL 2100F TEM/STEM and spectrum images were collected to investigate morphologies, size distribution and oxidation states of ceria nanoparticles (CeO_2-MNPs) in rat spleen tissue. A therapeutic dose (4 g/kg) of ~15–20 nm CeO_2-MNPs was used and instilled four times over a 2 week time period. The hydrothermal synthesis procedure for the CeO_2-MNPs resulted in a narrow size range ~20 nm [47]. The particle surfaces were capped using a citrate coating (10 %) in 5 % aqueous dispersion. The (CeO_2-MNPs) synthetic identity included size, surface charge (Zeta potential: −40 mV at pH 7.3) and structural characterization using HRTEM/STEM analyses and EELS in the spleen tissue (Fig. 4.9).

Previously, the *in vivo* processing, transformation and subcellular effects of CeO_2-MNPs in a rat model using a single high dose (85 mg/kg) was presented with corresponding effects on oxidative stress increases and decreases and internalized CeO_2-MNPs were shown to cause distinct cellular responses and oxidative stress, but also presented significant *in vivo* processing which releases smaller CeO_2-MNPs clouds with much improved ROS potential [27, 32]. Since CeO_2-MNPs can do both generate and scavenge free radical oxygen species (ROS), it is important to distinguish CeO_2-MNPs that contribute to either ROS production or ROS scavenging in subcellular levels [41]. Example II shows how ceria MNPs translocate to spleen tissue and in the spleen the original CeO_2-MNPs produced Ce-clouds (Fig. 4.9). In this particular case a therapeutic dose (4 g/kg) of CeO_2-MNPs not only bio- accumulated in spleen which can be demonstrated with the help of HRTEM and Dark Field STEM imaging, but the original ceria nanoparticles were also structurally altered and second generation plumes of ultra-fine (<3 nm) ceria nanoparticles formed close by, which can be seen as clouds next to the *in vivo* processed ceria precursors (Fig. 4.9). Corresponding EELS analyses along the EELS-trace line in Fig. 4.9 compare the redox state of the precursor and newly precipitated ceria clouds. The high angle STEM analysis along the EELS line profile used a small probe size (0.2 nm) to minimize any fixed tissue sample damage that could occur under the prolonged electron beam exposure. The oxidation states of Ce were determined by the fine structures of M4,5 edges in EELS as described elsewhere in details [77]. The schematic in Fig. 4.10 gives some insights on how to compute the EELS edges for Ce and, in particular, the energy loss for Ce M_4 versus Ce M_5. The greater the contribution of Ce M5, the higher is the ceria reduction potential [77]. Interestingly, the same kind of Ce-cloud formation was also shown previously for a high-dose of CeO_2-MNPs after intravenous uptake and sequestration of CeO_2-MNPs in liver and was associated with a much improved ROS potential [27]. Different valance states of the ultra-small CeO_2-MNPs needles are characterized by core loss EELS to have very high Ce^{+3} signatures (corresponding to oxygen vacancies) as evidenced by the greater Ce M_5 contributions obtained via the EELS analyses and are similar to those in the Ce-clouds (Fig. 4.9). Both HRTEM and Dark Field

STEM demonstrate that Ce-phosphates formed in the spleen and this typically occurs in lysosomal regions where ultra-small ceria particles transform/reform (the mechanism of transformation/reformation is not known at this time) (Figs. 4.11 and 4.12).

Elemental maps can be produced from EDS and EELS spectrum images (in high resolution STEM mode) and in the example below span across the regions where the Ce-nanoparticles accumulate. This information can then be used to build a thorough understanding of the temporal, structural and cellular relationships involving tissue composition and location of nanoparticles. An example is shown in Fig. 4.13 where elemental maps were generated over a select region that is illustrated using dark field STEM in 4.12. These are fairly low EELS pixel count maps in order not to destroy the tissue structures during the prolonged electron beam scanning. Therefore, a low angle dark field STEM condition has to be selected to bring out the cellular structures in the spleen (Fig. 4.13) while simultaneously analyzing the relative elemental composition and spectral signatures of for example Ce, P, C, Ca, N and O in the same region using STEM spectrum imaging (Fig. 4.13).

Elemental maps obtained from the EDS and EELS spectrum images allow for a comparison of the elemental distribution that is associated with the cellular structures and that of the accumulated nanoparticles. The low pixel count maps take about 30 min to acquire. Higher pixel count maps can be obtained but the required time increases rapidly and this can affect the beam/sample interaction and lead to artifacts. Elemental imaging may also be accomplished using an EELS imaging filter. Typically an in-column filter is more successful on biological specimens due to the smaller beam dose required. When using post column filters the sample stability may be impacted due to the high brightness required (electron intensity). The elemental imaging for Ce-MNPs that seem to preferentially locate around globular lipid-based components (Figs. 4.12 and 4.13) clearly shows that the Ca and N are highly enriched as part of the internal composition of the lipid structures and they have an outer shell or corona that is phosphor rich (P signal is high at the outside of the globular structures in Fig. 4.13). The Ce signal completely overlaps with the P signal suggesting, at the least, a spatial relationship. In case of the preferential Ce deposition at the outside of the lipid structures it would suggest that there is either a mechanism that controls the delivery of the Ce-MNPs to that particular P-rich location or, that Ce ions migrated to that region and formed new Ce-oxides, Ce-hydroxides or Ce-phosphates. The O-signal clearly shadows the areas of both, Ce and P signals (Fig. 4.13). The elemental map of the S-signal shows that it is confined to the lipid structures only. At this time it is not known how certain regions in cells govern nanoparticle delivery and accumulation, but there seems to be an underlying chemical control that needs to be considered. Much work will be required to understand the relationship between tissue components and nanoparticles, but the use of HRTEM/STEM and EELS is certainly a tool that will be very useful towards that goal. How the MNPs' port-of-entry, dose, exposure duration and post-exposure time factor into the transport phenomena, particle transformation and *in vivo* processing mechanisms is not known at this time.

4.3.4 Example III: Ferritin Nanoparticles Inside Lung and Liver Tissue

The uptake and sequestration of MNPs, both silica (amorphous SiO_2) and ceria (CeO_2) results in the partial breakdown and *in vivo* processing of the original MNP-particles as discussed in Examples I and II in earlier sections in this Chapter. Remarkably, there is additional evidence one can gain from HRTEM: the presence of different MNPs (SiO_2, CeO_2) in different organs (lung, liver, spleen) after being delivered via different uptake routes (inhalation, intravenous), have at least one response in common, specifically, the simultaneous formation of ferritin nanoparticles in the vicinity of the invader MNPs. Ferritins represent bio-mineralized iron nanoparticles that are typically 5–8 nm in size and trapped inside the cage of the iron storage protein [8]. They occur immediately juxtaposed to the cell-invading and inflammation-inducing MNPs [27]. Moreover, the ferritin nanoparticles are highly concentrated next to the MNPs when compared to tissue regions that are not affected by inflammation, as shown in the Dark Field STEM images in Figs. 4.14 and 4.15. The individual solitary bright white spots surrounding the invader MNPs (inside the lysosomal regions) each represent one ferritin nanoparticle of 5–8 nm size (Figs. 4.14 and 4.15). It is well established that ferritin nanoparticles form during the bio-mineralization of ferrous (reduced) iron. A conserved iron-binding site, the ferroxidase center of the ferritin protein regulates iron storage in iron metabolism [38]. It is generally assumed that ferrous iron Fe(II) binds the ferroxidase center and the oxidized iron Fe(III) spontaneously enters the ferritin cage. High resolution imaging as well as spectroscopic and kinetic studies of ferritins (family of 24 iron storage proteins), suggest many common characteristics, including highly symmetric subunits of a cavity-engulfing protein coating in which the iron bio-mineralization takes place. Furthermore, there are four channel passages through the protein shell that help facilitate ingress and egress of ions which results in an iron core with eight subunits rather than a single dense sphere [75]. There are catalytic sites at the inner shell “ferroxidase center” which control the oxidation of Fe(II). The mechanisms of biomineralization of iron that result in ferritin nanoparticles like the ones shown in Figs. 4.14 and 4.15 are described elsewhere [8, 38], but the association (close locality) with invader MNPs is novel and requires a thorough investigation of the subcellular mechanisms and participation of iron as a redox mediator to counter the effects of invader MNPs. The significance of iron in biological systems is due to its ability to engage in redox reactions, including the scavenging of free radicals [27]. In general, iron forms a labile iron pool that includes iron atoms, but free Fe(II) must be managed either by use in hemoglobin or inside of the iron storage protein, ferritin. Otherwise, reduced Fe(II) iron can participate in the Fenton reaction and cause free radical formation [44]. There are numerous transferrin receptors, all of which are proteins that participate in iron transport at the cellular and subcellular levels. Once Fe(II) is sequestered in the ferric form within the ferritin protein shell, this particular iron will not participate in free radical formation. In fact, the oxidation of one Fe(II) to Fe(III) releases an electron that can neutralize a free radical species and, thereby, act as an anti-oxidant. Each ferritin cavity can hold up to 4500 oxidized iron atoms [63] and each one had to release an electron while being oxidize. It is this catalytic process that provides ferritin with the anti-oxidant property. The physical characterization of the ferritin particles includes details of the protein shell as well as characterization of the mineralized iron oxide core. In the high resolution dark field images of the lung and spleen thin sections only the iron oxide core is visible due to the comparatively high atomic number

and close packing of the iron atoms, while the surrounding ferritin-protein shell has about the same density and general chemical make up as the cellular matrix and, therefore, is difficult to distinguish (Figs. 4.14 and 4.15). The dense iron core allows z-contrast imaging using HAADF-STEM (Figs. 4.14 and 4.15). When using aberration corrected STEM this technique provides insights into the detailed morphologies and structures of the iron core [70]. Although the exact composition and stoichiometry of the core is not well understood yet, most literature today suggests that the core is composed of a ferrihydrite (iron-oxyhydrite) and also approximates this structure in human liver [63].

The copious ferritin nanoparticles that form halos around sequestered MNPs (Figs. 4.14 and 4.15) occur in such a high concentration that it, unmistakably, seems to be a direct response to the presence (invasion) of the MNPs in either the lung or spleen (Figs. 4.14 and 4.15). Ferritin nanoparticles are typically present throughout cells, but not in the particularly high concentration that is shown inside the ferritin-halos around MNPs (Figs. 4.14 and 4.15). Unexpectedly, the elevated ferritin nanoparticle accumulation seems independent of the nature of the MNPs (amorphous SiO_2, CeO_2 and others not shown in this Chapter). The mechanisms that control the abundant *in vivo* formation of ferritin nanoparticles next to the invader MNPs need to be further investigated, but it seems to indicate that the cellular and subcellular response mechanism(s) trigger an upregulation of iron immediately juxtaposed to the MNPs. This is very important since MNPs are linked to inflammatory processes and possible cell toxicity, which results in formation of free radicals [44]. Either the MNPs or the free radicals, or both, initiate mechanisms that trigger the upregulation of iron in the same regions. Consequently, ferritin nanoparticles that form as a result of the oxidation of Fe(II) to Fe(III) can participate in free radical scavenging processes as mentioned earlier and provide the needed anti-oxidant response to counteract invader MNPs. This can explain the ferritin-rich halos that are observed in the HAADF-STEM images around the MNPs (Figs. 4.14 and 4.15). At this time there is no available data on a nanoparticle induced dose-dependent ferritin response, but it seems logical that the higher the MNPs dose, the greater the ferritin nanoparticle concentrations would be in the affected tissue regions.

4.4 Synchrotron Analysis: Dose-Dependent Nanoparticle Signatures in Tissue

X-ray absorption spectroscopy methods making use of synchrotron radiation, such as XANES and EXAFS, may prove useful in providing information on the electronic and local atomic structure of elements in nanotoxicology. A screening of selected tissue samples for elements of interest may provide information regarding the incorporation of such elements from exposure to nanoparticles as a function of a particular dose that led to a certain pathological response. An important analogy is when an X-ray absorption spectroscopy survey was conducted on coal samples to determine the chemical nature and structure of elemental impurities. In that case, the researchers were faced with a similar staggering problem. Coal contains nearly the entire periodic table as impurity elements, and many of the impurity elements were of concentrations 1000 ppm or less, which could not be confidently characterized by conventional microscopic, spectroscopic, or diffraction techniques [82]. Using predominantly fluorescence mode, significant and important

information was obtained on numerous trace elemental impurities in coal using X-ray absorption spectroscopy [37]. Just below the edge energy and prior to the single scattering region, pre-edge features provide useful information on site symmetry (e.g., a sharp feature is typically produced with tetragonal symmetry, while octahedral generally produces a faint signal), the white line region provides information on the oxidation state of the material, and the multi-scattering region provides information on the immediate environment of neighboring atoms. The higher energy region provides a wealth of information on the identity of neighboring atoms, their interatomic distances, and their degree of coordination. Although XANES in principal can also be obtained in high resolution STEM mode using electron microscope applications, elemental dispersion over larger tissue areas is not possible using large magnification settings and needs to be done at a synchrotron source. Two examples related to catalyst particles (iron oxide and ceria nanoparticles) that are often examined with regards to their nano-toxic response are provided below. In the first case [68] the role of the element K in promoting the carburization rate of iron oxide in Fischer-Tropsch synthesis catalysts was explored by XANES and EXAFS spectroscopy. The XANES spectra were recorded with the catalyst heated in flowing carbon monoxide (Fig. 4.16a). Changes in the white line are evident (Fig. 4.16a), and in comparing the spectra to those of reference compounds, reduction was found to proceed by way of Fe_2O_3 to Fe_3O_4 to FeO to Fe carbides. Simultaneous EXAFS spectra were recorded (Fig. 4.16b). The low distance- peak of Fe-O coordination and the high distance peak of Fe-Fe coordination in Fe_2O_3 change to match the distances of Fe-O and Fe-Fe coordination in Fe_3O_4. At the end of the trajectory, Fe-C bonds in Fe carbides are clearly observed in the intermediary range of distance. Thus, the two techniques (XANES and EXAFS) provided similar information on the chemical changes occurring, but simultaneously and from two different perspectives. Bio- mineralized iron oxides are very often present at the cellular and subcellular levels and it is important to distinguish oxidation states and also to observe whether iron may be coordinated to carbon, sulfur or phosphor and if variations occur as a function of dose (nanoparticle exposure).

A second example [45], on the doping of nanosized ceria (CeO_2) domains with platinum doping of 0.5 % (by weight) and 50 % (by mole) calcia, is described below. The XANES patterns of Ce^{4+} and Ce^{3+} are very different (Fig. 4.17a).

where Ce^{4+} contains two very broad peaks, as well as additional features, while Ce^{3+} exhibits a sharp distinct peak, B_0. This is based on changes in the electronic structure of ceria, and its effect on the allowed electronic transitions. When the same CeO_2 nanoparticle catalyst was heated in hydrogen (Fig. 4.17b) to activate the surface by reduction, the addition of the dopants (Pt and Ca) facilitated surface shell reduction to ~200°C (from 450 to 500°C for undoped ceria), and bulk reduction commenced at ~400°C (rather than >700°C for undoped ceria). This clearly demonstrates the sensitivity of the analysis tool towards elemental, structural and thermal changes as a function of reduction potential. Thus, using high intensity X-rays generated at the synchrotron can provide a wealth of information regarding the identity, chemical state, and local atomic structure of nanoparticles, and may provide key information in any survey of tissue samples for nanotoxicology.

4.5 Synopsis

In this chapter the inter-relationship between dose, nanoparticle uptake, cellular and subcellular interactions and nanotoxicity has been discussed with examples of means of observation of *in vivo* bio-processing and response. Emphasis is placed on the importance of the precision of characterization of the starting particles, the particles in a biological environment, and the physiological response. The relationship between dose, bio-processing, and response is an area of active research as all three may be related in a non-linear manner. It is pointed out that relatively insoluble materials like CeO_2 have been observed *in vivo* to undergo significant changes in shape, size, material phase and electronic structure. Because of this, the modelling and prediction of dose versus toxicity over time becomes a non-linear problem because the initial particles can transform over time and initiate different responses that evolve as the dynamic system undergoes further transformations. The examples in this chapter illustrate two advanced materials characterization methods that are useful in the characterization of nanoparticles, before and after introduction in the biological environment, and in observing specific types of physiological response. These methods are advanced analytical electron microscopy (STEM/EELS) and x-ray absorption near edge spectroscopy (XANES). In conclusion the dose response relationship is complicated by the physicochemical transformations in the nanoparticles induced by the biological system producing an altered response. Thus, the modelling and prediction of dose-response-toxicity relationships has to take into account non-linear dependencies when attempting to predict a dose versus toxicity response relationship. This has to be especially considered when predictive modelling of nanomaterials utilizes *in vitro* models. Therefore, the long-term goal is to develop cellular in vitro models that can support dynamic processing of nanoparticles for exposure risk assessment.

References

1. Altavilla C, Ciliberto E (eds) (2010) Inorganic Nanoparticles Synthesis, Applications, and Perspectives. CRC Press, Boca Raton, Florida, p 576 Print ISBN: 978–1-4398-1761-2, eBook ISBN: 978-1-4398-1762-9
2. Anderson SC, Birkeland CR, Anstis GR, Cockayne DJH (1997) An approach to quantitative compositional profiling at near atomic resolution using high-angle anular dark-field imaging. Ultramicroscopy 69:83–103
3. Bates ME, Keisler JM, Zussblatt NP, Plourde KJ, Wender BA, Linkov I (2015) Balancing research and funding using value of information and portfolio tools for nanomaterial risk classification. Nat Nanotechnol 9:249
4. Baisch BL, Corson NM, Wade-Mercer P, Gelein R, Kennell AJ, Oberdörster G, Elder A (2014) Equivalent titanium dioxide nanoparticle deposition by intratracheal instillation and whole body inhalation: the effect of dose rate on acute respiratory tract inflammation. Part Fibre Toxicol 11(5): 16 PMCID:PMC3905288 [PubMed: 24708749]
5. Bermudez E, Mangum JB, Wong BA, Asgharian B, Hext PM, Warheit DB, Everitt JI (2004) Pulmonary responses of rats, mice, and hamsters to subchronic inhalation of ultrafine titanium dioxide particles. Toxicol Sci 77:347–357 [PubMed: 14600271]
6. Bilberg K, Hovgaard MB, Besenbacher F, Baatrup E (2012) In vivo toxicity of silver nanoparticles and silver ions in zebrafish (Danio rerio). J Toxicol 2012:9 Article ID 283784
7. Bonner JC, Silva RM, Taylor AJ, Brown JM, Hilderbrand SC, Castranova V, Porter D, Elder A, Oberdörster G, Harkema J, Bramble L, Kavanagh TJ, Botta D, Nel A, Pinkerton KE (2013)

Interlaboratory evaluation of rodent pulmonary responses to engineered nanomaterials. Environ Health Perspect 121:676–682 PMC3672912 [PubMed: 23649427]

8. Bradley JM, Moore GR, LeBrun NE (2014) Mechanisms of iron mineralizaiton in ferritins: one size does not fit all. J Biol Inorg Chem 19(6):775–785. doi:10.1007/s00775-014-1136-3 [PubMed: 24748222]
9. Brunner TJ, Wick P, Manser P, Spohn P, Grass RN, Limbach LK, Bruinink A, Stark WJ (2006) In vitro cytotoxicity of oxide nanoparticles: comparison to asbestos, silica, and the effect of particle solubility. Environ Sci Technol 15(4D(14)):4374–4381
10. Burello E, Worth AP (2011) A theoretical framework for predicting the oxidative stress potential of oxide nanoparticles. Nanotoxicol 5(2):228–235
11. Buzea C, Blandino IIP, Robbie K (2007) Nanomaterials and nanoparticles: sources and toxicity. Biointerphases 2(4):MR17–MR172 [PubMed: 20419892]
12. Crosera M, Bovenzi M, Maina G, Adami G, Zanette C, Florio C, Larese FF (2009) Nanoparticle dermal absorption and toxicity: a review of the literature. Int Arch Occup Environ Health 82(9): 1043–1055 [PubMed: 19705142]
13. DeSouza PM, Neto RCR, Borges LEP, Jacobs G, Davis BH, Graham UM, Resasco D, Noronha FB (2015) Effect of zirconia morphology on hydrogenation of phenol over Pd/ZrO2. ACS Catal 5(12): 7358
14. Docter D, Strieth S, Westmeier D, Hayden O, Gao M, Knauer SK, Stauber RH (2015) No king without a crown – impact of the nanomaterial-protein corona on nanobiomedicine. Nanomedicine (London) 10(3):503–519
15. Driscoll KE (1996) Role of inflammation in the development of rat lung tumors in response to chronic particle exposure. Inhal Toxicol 8(Suppl):139–153
16. Egerton RF (2011) Electron energy loss in the electron microscope, 3rd ed. Springer, New York ISBN 978-1-4419-9582-7
17. Elder ACP, Gelein R, Finkelstein JN, Cox C, Oberdörster G (2000) The pulmonary inflamma-tory response to inhaled ultrafine particles is modified by age, ozone exposure, and bacterial toxin. Inhal Toxicol 12(Suppl. 4):227–246 [PubMed: 12881894]
18. Elder A, Gelein R, Finkelstein JN, Driscoll KE, Harkema J, Oberdörster G (2005) Effects of subchronically inhaled carbon black in three species. I. Retention kinetics, lung inflammation, and histopathology. Toxicol Sci 88(2):614–629 [PubMed: 16177241]
19. Elder A, Couderc JP, Gelein R, Eberly S, Cox C, Xia X, Zareba W, Hopke P, Watts W, Kittelson D, Frampton M, Utell M, Oberdörster G (2007) Effects of on-road highway aerosol exposures on autonomic responses in aged, spontaneously hypertensive rats. Inhal Toxicol 19:1–12 [PubMed: 17127638]
20. Elder A, Vidyasagar S, DeLouise L (2009) Physicochemical factors that affect metal and metal oxide nanoparticle passage across epithelial barriers. Wiley Interdiscip Rev Nanomed Nanobiotechnol 1(4):434–450.4004356 [PubMed: 20049809]
21. Fawcett DW (1966) An atlas of fine structure: the cell, its organelles, and inclusions. W.B. Saunders, Philidelphia
22. Feynman RP (1960) There's Plenty of Room at the Bottom. Eng Sci 23(5):22–36
23. Foroozandeh P, Aziz AA (2015) Merging worlds of nanomaterials and biological environment: factors governing protein corona formation on nanoparticles and its biological consequences. Nanoscale Res Lett 10:221 4437989 [PubMed: 25995715]
24. Fruijtier-Polloth C (2012) The toxicological mode of action and the safety of synthetic amorphous silica – A nanostructured material. Toxicology 284(2):61–70. doi:10.1016/j.tox.2012.02.001
25. Gebauer JS, Malissek M, Simon S, Knauer SK, Maskos M, Stauber RH, Peukert W, Treuel L (2012) Impact of the nanoparticle-protein corona on colloidal stability and protein structure. Langmuir 28(25):9673–9679 [PubMed: 22524519]
26. Graham UM, Khatri RA, Dozier A, Jacobs G, Davis BH (2009) 3D ridge-valley structure of a Pt ceria catalyst: HRTEM and EELS spectrum imaging. J Cat Lett 132(2):335–341
27. Graham UM, Tseng MT, Jasinski JB, Yokel RA, Unrine JM, Davis BH, Dozier AK, Hardas SS, Sultana R, Grulke EA, Butterfield DA (2014) In vivo processing of ceria nanoparticles inside liver:

impact on free-radical Scavenging activity and oxidative stress. Chempluschem 79(8):1083–1088.4551665 [PubMed: 26322251]

28. Graham UM, Dozier AK, Wang C, Tseng MT, Fernbeck JE, Birch ME, Davis BH (2015) Observations of in vivo processing of metal oxide nanoparticles by analytical TEM/STEM. Microsc Microanal:2287, 21, (Suppl 3)
29. Grosse S, Haugland HK, Lilleng P, Ellison P, Hallan G, Hol PJ (2015) Wear particles and ions from cemented and uncemented titanium-based hip prostheses-a histological and chemical analysis of retrieval material. J Biomed Mater Res B Appl Biomater 103(3):709–717. 4413358 [PubMed: 25051953]
30. Gulson B, McCall MJ, Bowman DM, Pinheiro T (2015) A review of critical factors for assessing the dermal absorption of metal oxide nanoparticles from sunscreens applied to humans, and a research strategy to address current deficiencies. Arch Toxicol 89(11):1909–1930 [PubMed: 26140917]
31. Hajarul AAW, Nor DZ, Aziz AA, Razak KA (2012) Properties of amorphous silica entrapped isoniazid drug delivery system. Adv Mat Res 364:134–138
32. Hardas SS, Sultana R, Warrier G, Dan M, Wu P, Grulke EA, Tseng MT, Unrine JM, Graham UM, Yokel RA, Butterfield DA (2013) Rat hippocampal responses up to 90 days after a single nanoceria dose extends a hierarchical oxidative stress model for nanoparticle toxicity. Nanotoxicol 8(Suppl. 1):155–166
33. Hartland A, Lead JR, Slaveykova VI, O'Carroll D, Valsami-Jones E (2013) The environmental significance of natural nanoparticles. Nat Educ Knowl 4(8):7
34. Heinrich U, Fuhst R, Rittinghausen S, Creutzenberg O, Bellmann B, Koch W, Levsen K (1995) Chronic inhalation exposure of Wistar rats and two different strains of mice to diesel engine exhaust, carbon black, and titanium dioxide. Inhal Toxicol 7:533–556
35. Hellmann R, Cotte S, Cadel E, Malladi S, Karlsson LS, Lozano-Perez S, Cabie M, Seyeux A (2015) Nanometre-scale evidence for interfacial dissolution-reprecipitation control of silicate glass corrosion. Nat Mater 14(3):307–311 [PubMed: 25559424]
36. Hirsch PB, Howie A, Whelan MJ (1962) On the production of X-rays in thin metal foils. Philos Mag 7:2095–2100
37. Hodgson KO, Hedman B, Penner-Hahn JE (eds) (1984) EXAFS and near edge structure III, Proc In Physics 2, Springer, Berlin/Heidelberg GmbH
38. Honarmand Ebrahimi K, Bill E, Hagedoorn PL, Hagen WR (2012) The catalytic center of ferritin regulates iron storage via Fe(II)-Fe(III) displacement. Nat Chem Biol 8(11):941–948. doi:10.1038/nchembio.1071 [PubMed: 23001032]
39. Jones JR (2013) Review of bioactive glass: from Hench to hybrids. Acta Biomater 9(1):4457–4486 [PubMed: 22922331]
40. Keller J, Wohlleben W, Ma-Hock L, Strauss V, Gröters S, Küttler K, Wiench K, Herden C, Oberdörster G, Van Ravenzwaay B, Landsiedel R (2014) Time course of lung retention and toxicity of inhaled particles: short-term exposure to nano-ceria. Arch Toxicol 88(11): 2033–2059 [PubMed: 25273020]
41. Kim CK, Kim T, Choi IY, Soh M, Kim D, Kim YJ, Jang H, Yang HS, Kim JY, Park HK, Park S, Yu T, Yoon BW, Lee SH, Hyeon T (2012) Ceria nanoparticles that can protect against ischemic stroke. Angew Chem Int Ed Eng 51:11039
42. Kreyling WG, Semmler-Behnke M, Seitz J, Scymczak W, Wenk A, Mayer P, Takenaka S, Oberdörster G (2009) Size dependence of the translocation of inhaled iridium and carbon nanoparticle aggregates from the lung of rats to the blood and secondary target organs. Inhal Toxicol 21(Suppl. 1):55–60
43. Krug HF (2014) Nanosafety research – are we on the right track. J Angew Chemie 53(46):12304–12319
44. Lemire JA, Harrison JJ, Turner RJ (2013) Box 3: the Fenton reaction, free radical chemistry and metal poisoning. Nat Rev Microbiol 11:371–384. doi:10.1038/nrmicro3028 [PubMed: 23669886]
45. Linganiso L, Pendyala V, Jacobs G, Davis B, Cronauer D, Kropf A, Marshall C (2011) Low-temperature water-gas-shift: doping ceria improves reducibility and mobility of O-bound species and catalyst activity. Cat Letters 141(12):1723

46. Loane RF, Kirkland EJ, Silcox J (1988) Visibility of single heavy atoms on thin cyrstalline silicon in simulated annular dark-field STEM images. Acta Crystallogr A 44:912–927
47. Mai HX, Sun LD, Zhang YW, Si R, Feng W, Zhang HP, Liu HC, Yan CH (2005) Shape- selective synthesis of oxygen storage behavior of ceria nanopolyhedra, nanorods and naocubes. J Phys Chem B 109(51):24380–24385. doi:10.1021/jp055584b [PubMed: 16375438]
48. Maynard AD, Baron PA, Foley M, Shvedova AA, Kisin ER, Castranova V (2004) Exposure to carbon nanotube material: aerosol release during the handling of unrefined single-walled carbon nanotube material. J Toxicol Environ Health Part A 67(1):87–107 [PubMed: 14668113]
49. Massie I, Dziasko M, Kureshi A, Levis HJ, Morgan L, Neale M, Sheth R, Tovell VE, Vernon AJ, Funderburgh JL, Daniels JT (2015) Advanced imaging and tissue engineering of the human limbal epithelial stem cell niche. Methods Mol Biol 1235:179–202. doi:10.1007/978-1-4939-1785-3_15 [PubMed: 25388395]
50. Mercer RR, Scabilloni JF, Hubbs AF, Wang L, Battelli LA, McKinney W, Castranova V, Porter DW (2013) Extrapulmonary transport of MWCNT following inhalation exposure. Part Fibre Toxicol 10(38):13 [PubMed: 23587247]
51. Mortensen LJ, Ravichandran S, Delouise LA (2013) The impact of UVB exposure and differentiation state of primary keratinocytes on their interaction with quantum dots. Nanotoxicology 7:1244–1254 3779483 [PubMed: 22998293]
52. Mortensen LJ, Faulknor R, Ravichandran S, Zheng H, DeLouise LA (2015) UVB dependence of quantum dot reactive oxygen species generation in common skin cell models. J Biomed Nanotechnol 11(9):1644–1652 PMCID: PMC4625909 [PubMed: 26485933]
53. Muller DA, Sorsch T, Moccio S, Baumann FH, Evans-Lutterodt K, Timp G (1999) The electronic structure at the atomic scale of ultrathin gate oxides. Nature 399:758–761
54. Naess EM, Hofgaard A, Skaug V, Gulbrandsen M, Danielsen TE, Grahnstedt S, Skogstad A, Holm JO (2015) Titanium dioxide nanoparticles in sunscreen penetrate the skin into viable layers of the epidermis: a clinical approach. Photodermatol Photoimmunol Photomed 32(1):48–51 [PubMed: 26447850]
55. Nagashima K, Zheng J, Pamiter D, Patri AK (2011) Biological tissue and cell culture specimen preparation for TEM nanoparticle characterization. Methods Mol Biol 697:83–91. doi: 10.1007/978-1-60327-198-1_8 [PubMed: 21116956]
56. Nel A, Xia T, Mädler L, Li N (2006) Toxic potential of materials at the nanolevel. Science 311:622–627 [PubMed: 16456071]
57. Nellist PD, Pennycook SJ (2000) The principles and interpretation of annular dark-field Z contrast imaging. Advances Imaging Electron Phys 113:147–203
58. Oberdörster G, Finkelstein JN, Johnston C, Gelein R, Cox C, Baggs R, Elder ACP (2000) Acute pulmonary effects of ultrafine particles in rats and mice. Health Effects Institute, Cambridge, pp. 1–74
59. Oberdörster G (2002) Toxicokinetics and effects of fibrous and nonfibrous particles. Inhal Toxicol 14:29–56 [PubMed: 12122559]
60. Oberdörster G, Sharp Z, Atudorei V, Elder A, Gelein R, Kreyling W, Cox C (2004) Translocation of inhaled ultrafine particles to the brain. Inhal Toxicol 16(6–7):437–445 [PubMed: 15204759]
61. Oberdörster G, Oberdörster E, Oberdörster J (2007) Concepts of nanoparticle dose metric and response metric. Environ Health Perspect 115(6):A290 PMC1892118
62. Oberdörster G (2015) Predictive modeling of nanomaterial risk: combining or replacing in vivo with in vitro studies? CompNanoTox, 4 Nov, Malaga, Spain
63. Pan Y-H, Sader K, Powell JJ, Bleloch A, Gass M, Trinick J, Warley A, Brydson AR, Brown A (2009) 3D morphology of the human hepatic ferritin mineral core: new evidence for a subunit structure revealed by single particle analysis of HAADF-STEM images. J Struct Biol 166(1):22–31. doi:10.1016/j.jsb.2008.12.001 [PubMed: 19116170]
64. Pan H, Myerson JW, HU L, Marsh JN, Hou K, Scott MJ, Allen JS, Hu G, Roman SS, Lanza GM, Schreiber RD, Schlesinger PH, Wickline SA (2013) Programmable nanoparticle functionalization for in vivo targeting. FASEB 27(1):255–264
65. Pennycook SJ, Varela M (2011) New views of materials through aberration-corrected scanniung transmission electron microscopy. Microscopy 60(1):5213–5223

66. Ravichandran S, Mortensen LJ, DeLouise LA (2011) Quantification of human skin barrier function and susceptibility to quantum dot skin penetration. Nanotoxicol 5(4):675–686 PMID: 21142716

67. Rehr JJ, Kas JJ, Vila FD, Prange MP, Jorissen K (2010) Parameter-free calculations of X-ray spectra with FEFF9. Phys Chem Chem Phys 12(21):5503–5513. doi:10.1039/b926434e [PubMed: 20445945]

68. Ribeiro MC, Jacobs G, Davis BH, Cronauer DC, Kropf AJ, Marshall CL (2010) Fischer- Tropsch synthesis: deactivation as a function of potassium promoter loading for precipitated iron catalyst. J Phys Chem C 114:7895–7903

69. Rushton EK, Jiang J, Leonard SS, Eberly S, Castranova V, Biswas P, Elder A, Han X, Gelein R, Finkelstein J, Oberdorster G (2010) Concept of assessing nanoparticle hazards considering nanoparticle dosemetric and chemical/biological response metrics. J Toxicol Environ Health A 73(5):445–461 [PubMed: 20155585]

70. Sader K, Pan Y, Bleloch AL, Brydson R, Brown A (2008) Structural characterization of protein-caged iron minerals in biological systems. J. Physics: Conference Series 126(2008) 012006. doi: 10.1088/1742-6596/126/1/012006

71. Semmler M, Seitz J, Erbe F, Mayer P, Heyder J, Oberdörster G, Kreyling WG (2004) Long- term clearance kinetics of inhaled ultrafine insoluble iridium particles from the rat lung, including transient translocation into secondary organs. Inhal Toxicol 16:453–459 [PubMed: 15204761]

72. Sotiriou GA, Watson C, Murdaugh KM, Darrah TH, Pyrgiotakis G, Elder A, Brain JD, Demokritou P (2014) Engineering safer-by-design silica-coated ZnO nanorods with reduced DNA damage potential. Environ Sci Nano 1(2):144–153 PMC4060637 [PubMed: 24955241]

73. Surekha P, Kishore AS, Srinivas A, Selvam G, Goparaju A, Reddy PN, Murthy PB (2012) Repeated dose dermal toxicity study of nano zinc oxide with Sprague-Dawley rats. Cutan Ocul Toxicol 31(1):26–32 [PubMed: 21830917]

74. Tomer R, Ye L, Hsueh B, Deisseroth k (2014) Advanced clarity for rapid and high-resolution imaging of intact tissues. Nat Protoc 9:1682–1697. doi:10.1038/nprot.2014.123 [PubMed: 24945384]

75. Tosha T, Behera RK, Ng HL, Bhattasali O, Alber T, Theil EC (2012) Ferritin protein nanocage ion channels: gating by N-terminal extensions. J Biol Chem 287(16):13016–13025. doi:10.1074/jbc.M111.332734 [PubMed: 22362775]

76. Toumey C (2009) Plenty of room, plenty of history. Nat Nanotechnol 4:783–784 [PubMed: 19966818]

77. Turner S, Lazar S, Freitag B, Egoavil R, Verbeeck J, Put S, Strauven Y, VanTendeloo G (2011) High resolution mapping of surface reduction in ceria nanoparticles. Nanoscale 3(8):3385–3390. doi:10.1039/c1nr10510h [PubMed: 21720618]

78. Utembe W, Potgieter K, Stefaniak AB, Gulumian M (2015) Dissolution and biodurability: important parameters needed for risk assessment of nanomaterials. Part. Fibre Toxicol 12(11):12 [PubMed: 25944145]

79. Walkey CD, Chan WC (2012) Understanding and controlling the interaction of nanomaterials with proteins in a physiological environment. Chem Soc Rev 41(7):2780–2799 [PubMed: 22086677]

80. Wang W, McCool G, Kapur N, Yuan G, Shan B, Nguyen M, Graham UM, Davis BH, Jacobs G, Cho K, Hao X (2012) Mixed-phase oxide catalyst based on Mn-mullite (Sm, Gd)Mn2O5 for NO oxidation in diesel exhaust. Science 337(6096):832–835 [PubMed: 22904009]

81. Williams DB, Carter CB (2009) ISBN-10: 0387765026 Transmission electron microscopy a textbook for materials science, 2nd edn Springer, New York

82. Wong J, Lytle FW, Greegor RB, Maylotte DH, Lamson S, Glover B (1984) EXAFS and XANES studies of trace elements in coal, in EXAFS and Near Edge Structure III, Proc. in Physics 2. Hodgson KO, Hedman B, Penner-Hahn JE (eds), Springer Berlin, Heidelberg GmbH 1984, p 362–367

83. Wu J, Liu W, Xue C, Zhou S, Lan F, Bi L, Xu H, Yang X, Zeng FD (2009) Toxicity and penetration of TiO2 nanoparticles in hairless mice and porcine skin after subchronic dermal exposure. Toxicol Lett 191(1):1–8 [PubMed: 19501137]

84. Wu JS, Kim AM (2013) Imaging and elemental mapping of biological speciments with a dual-EDS dedicated scanning transmission electron microscope. Ultramicroscopy 128:24–31 [PubMed: 23500508]

85. Wu N, Xie Y, Nel A, Holian A (2013) Inter-laboratory comparison of in vitro nanotoxicological assays from the NIEHS NanoGo Consortium. Environ Health Perspect 121:683–690 PMC3672931 [PubMed: 23649538]

86. Yang H, Lozano JG, Pennycook SJ, Jones L, Hirsch PB, Nellist PD (2015) Imaging screw dislocations at atomic resolution by aberration-corrected electron optical sectioning. Nat Comm 6:7266. doi:10.1038/ncomms8266

87. Yokel RA, Au TC, MacPhail RC, Hardas SS, Butterfield DA, Sultana R, Goodman M, Tseng MT, Dan M, Haghnazar SS, Unrine JM, Graham UM (2012) Distribution, elimination, and biopersistence to 90 days of a systemically introduced 30 nm ceria-engineered nanomaterial in rats. Toxicol Sci 127(1):256–268 [PubMed: 22367688]

88. Zhang H, Ji Z, Xia T, Meng H, Low-Kam C, Liu R, Pokhrel S, Lin S, Wang X, Liao YP, Wang M, Li L, Rallo R, Damoiseaux R, Telesca D, Mädler L, Cohen Y, Zink JI, Nel AE (2012) Use of metal oxide nanoparticle band gap to develop a predictive paradigm for oxidative stress and acute pulmonary inflammation. ACS Nano 6(5):4349–4368 [PubMed: 22502734]

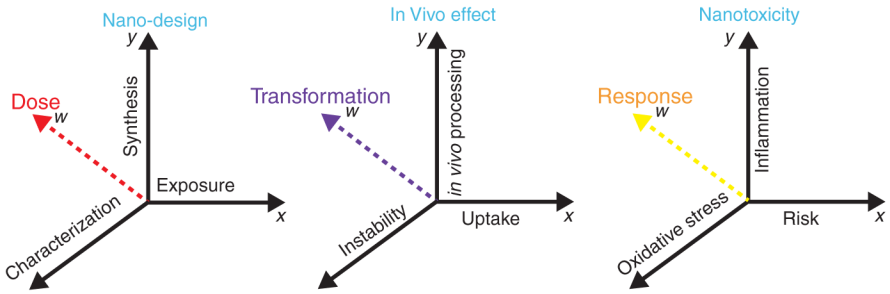

Fig. 4.1.

Schematic illustration of nanoparticle dose-dependent reactivity and physiological response

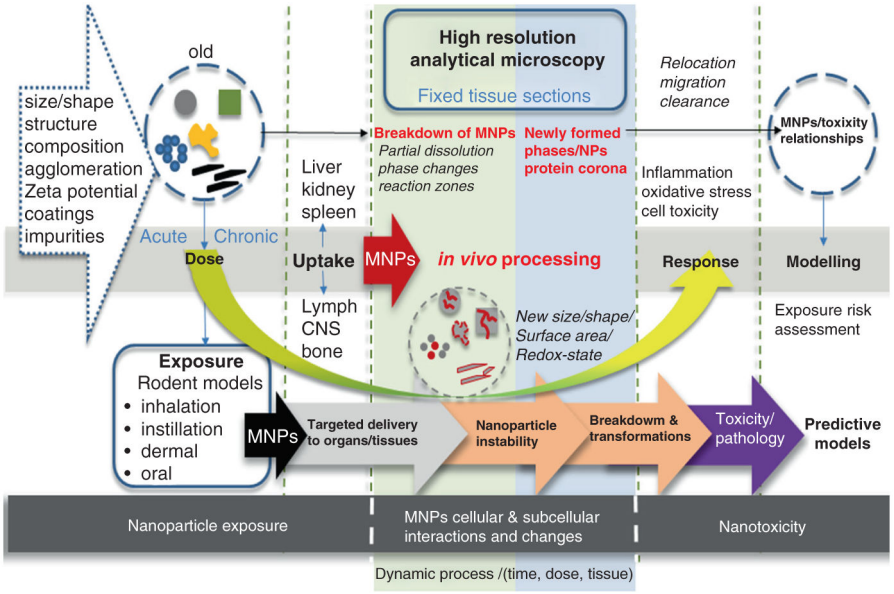

Fig. 4.2.

From dose to response: MNPs characterization, followed by dose-dependent exposure in rodent model, uptake into organs/tissues, *in vivo* processing and nanotoxicity assessment and modelling

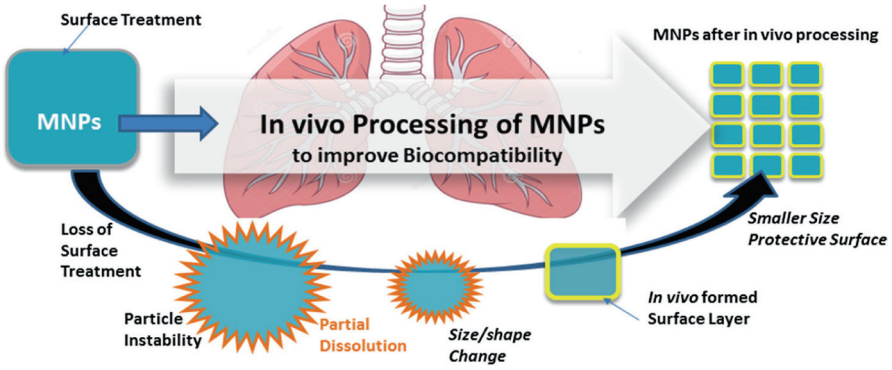

Fig. 4.3.

Nanoparticle breakdown can lead to improved biocompatibility

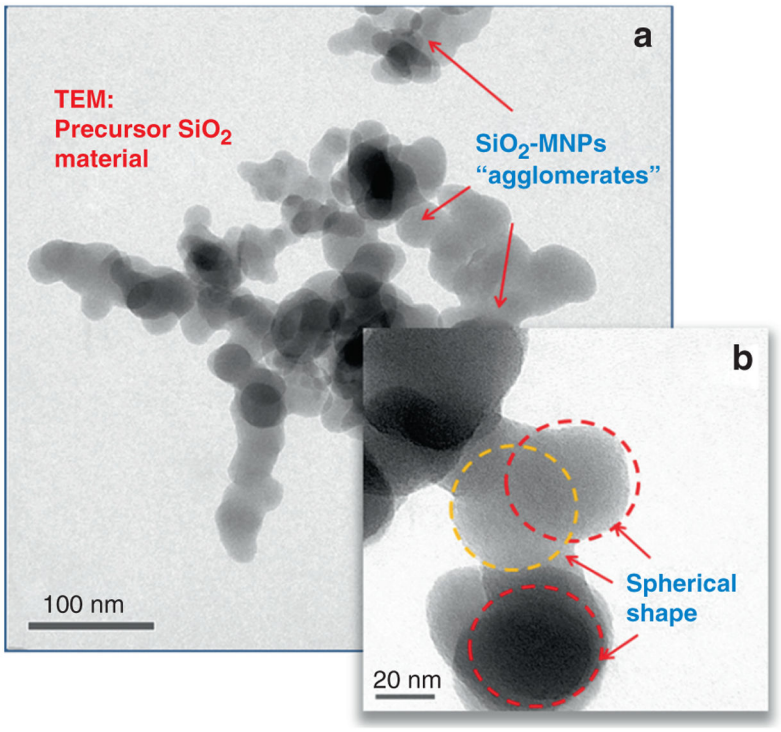

Fig. 4.4.

illustrates precursor SiO_2-MNPs prior to dose controlled inhalation into lungs. (**a**) Large agglomerates. (**b**) Precursor SiO_2-MNPs with amorphous nanostructures and predominantly *spherical shape*. Some *overlapping spheres* are marked with *circles*

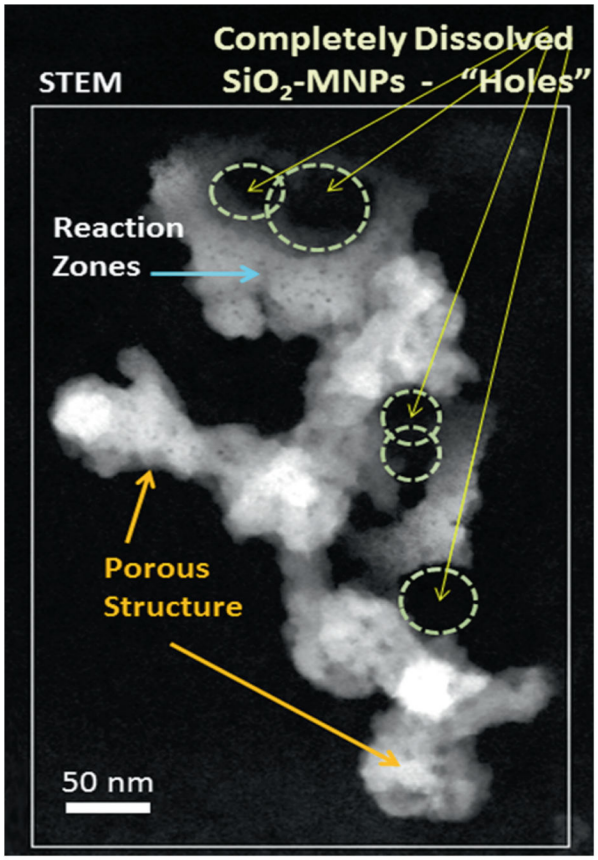

Fig. 4.5.

Dark field STEM imaging of lung section after repeated dose inhalation and 27 days post treatment. SiO_2-MNPs show pores and significant *in vivo* processing. Almost all of the original spherical morphology has disappeared after 27 days post treatment exposure. SiO_2-MNPs show dissolution patterns, void/pore formation (*yellow arrows*) and significant outward growth of reaction zones (secondary growth shown by *blue arrow*)

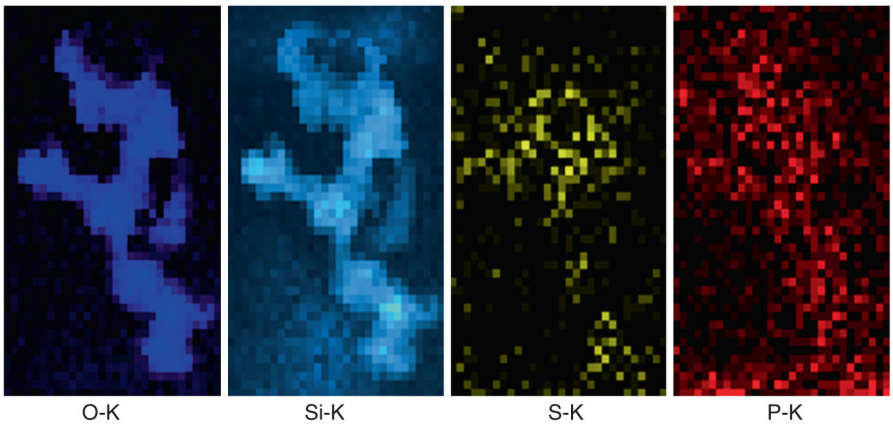

Fig. 4.6.
Elemental EDS maps of O, Si, S, and P taken from a region in Fig. 4.4

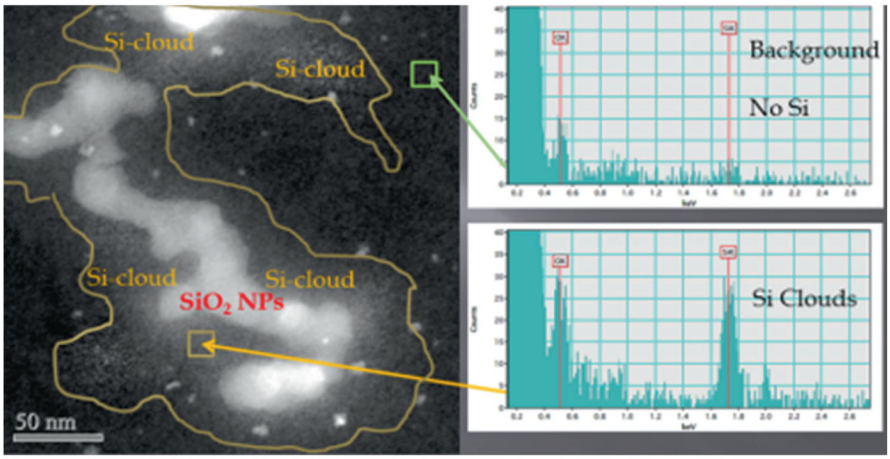

Fig. 4.7.

Dark Field STEM imaging and EDS spot analyses show the bioprocessing of SiO_2-MNPs in alveolar macrophages. Migration of Si occurred outwards and led to a secondary reaction zone “Si-cloud” between SiO_2-MNPs and yellow line. The small very bright spots in the Si-cloud region are ferritin nanoparticles

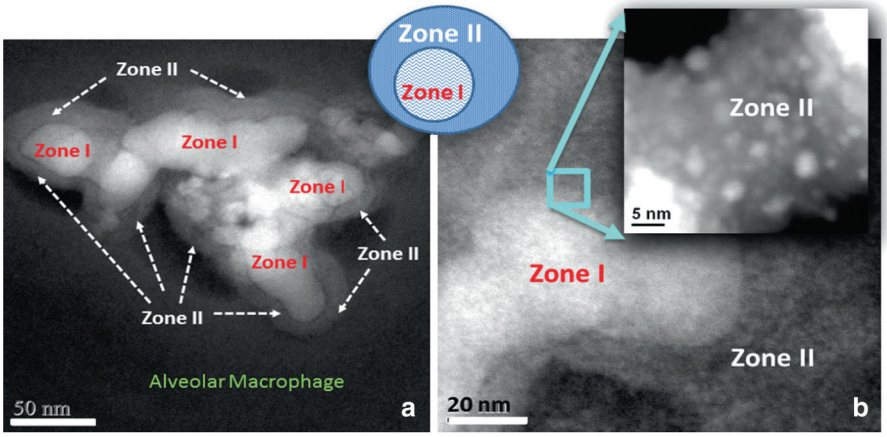

Fig. 4.8.

(**a**) Dark Field STEM image shows *in vivo* breakdown of SiO_2-MNPs in alveolar macrophage (Zone I) and formation of Zone II. (**b**) Magnified region shows small nanoparticles in Zone II

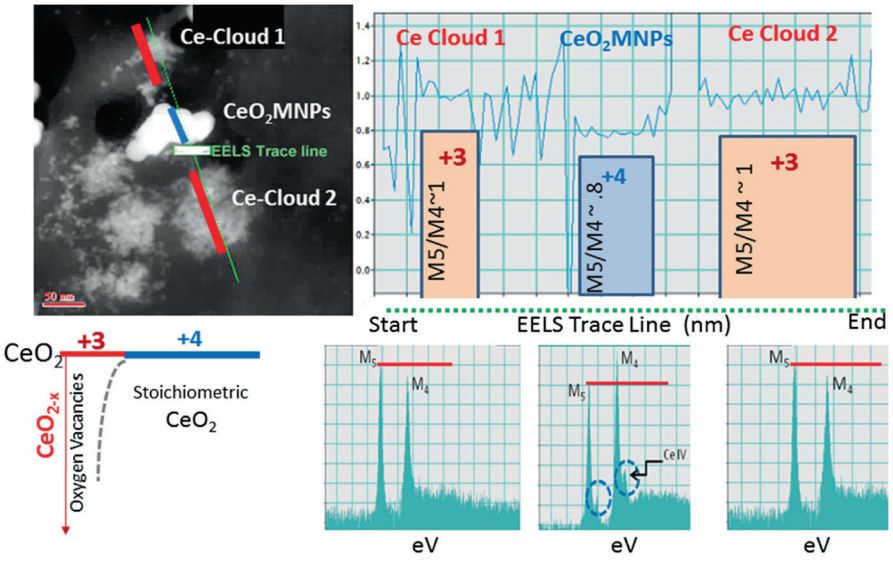

Fig. 4.9.

STEM and EELS analyses of CeO_2-MNPs in spleen after a therapeutic dose and 14 days residence time. Analysis of the ceria M5/M4 ratio along the line profile from an EELS spectrum image

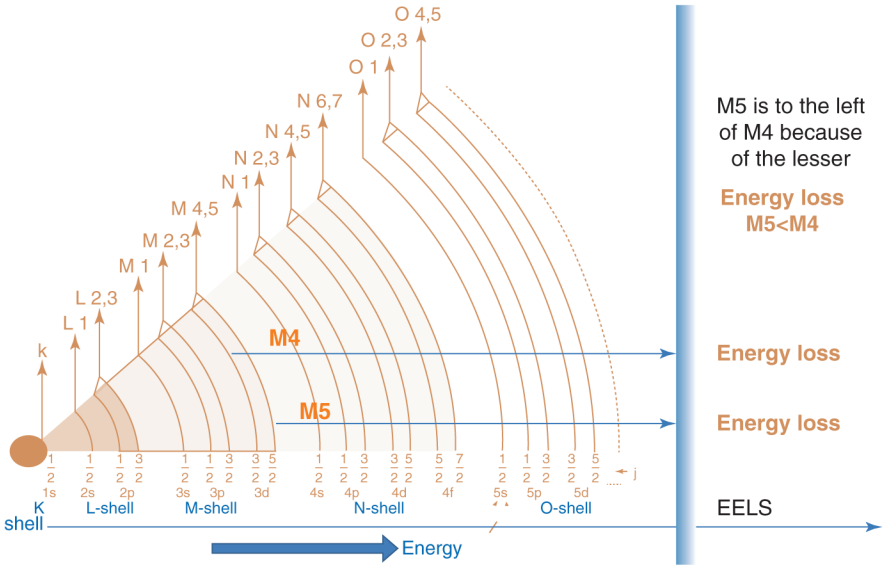

Fig. 4.10.

Schematic illustration of energy loss for computing EELS edges for Ce

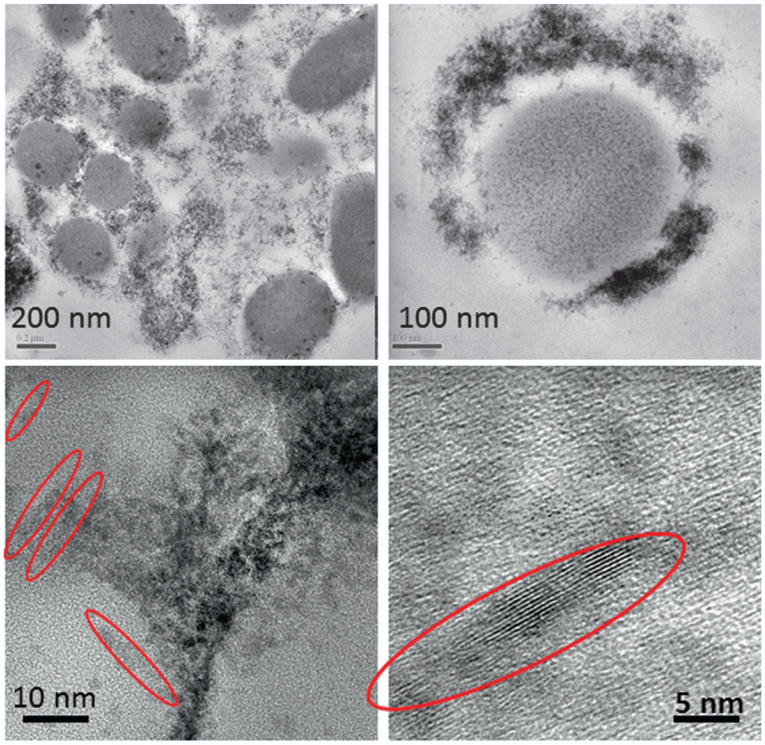

Fig. 4.11.

TEM and HRTEM images with increasing magnification show the presence of CeO_2-MNPs and Ce-phosphate after *in vivo* processing and leads to a local arrangement. Many MNPs are self- aligning to form needle- shaped structures indicted with *red arrows*

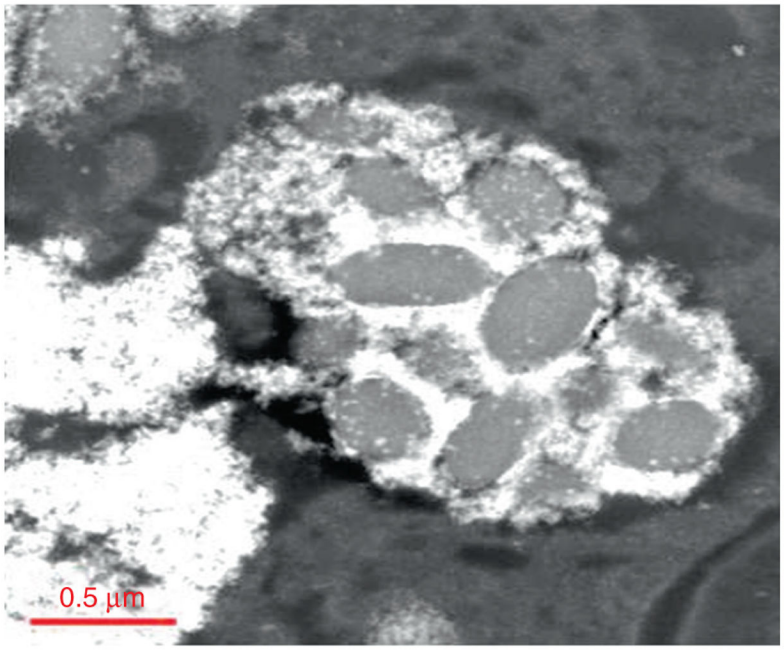

Fig. 4.12.

CeO2-MNPs are imaged using low angle dark field STEM condition showing cellular structures in the spleen. The CeO_2-MNPs localize around cellular inclusions

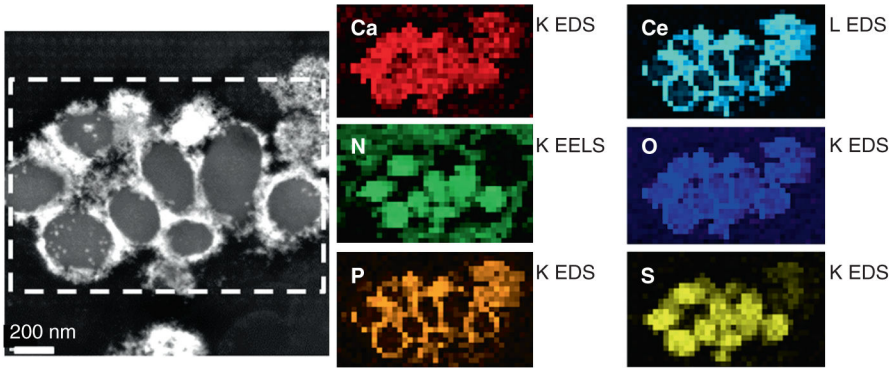

Fig. 4.13.

STEM spectrum imaging and elemental maps of Ce-MNPs localized around spleen inclusions

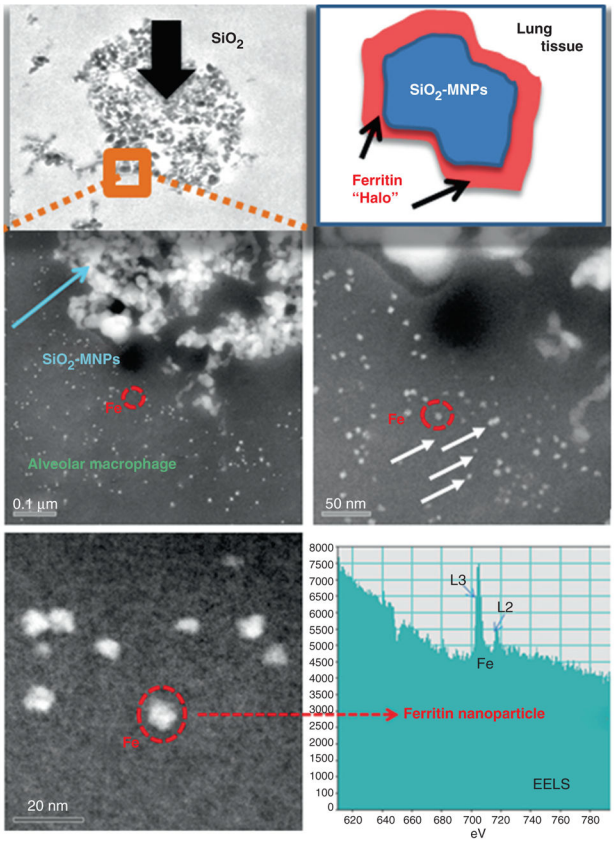

Fig. 4.14.

SiO_2-MNPs in TEM and dark field STEM showing cellular structure of the alveolar macrophage, location. The SiO_2-MNPs are surrounded by ferritin nanoparticle halos identified using EELS spot analysis

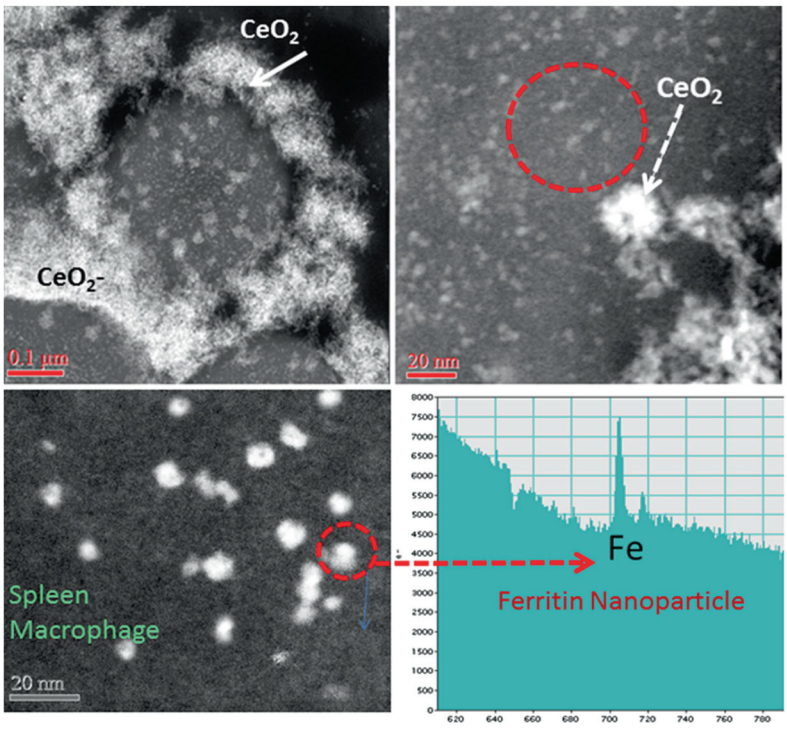

Fig. 4.15.

CeO_2-MNPs in dark field STEM showing cellular structure in the spleen macrophage. The CeO_2-MNPs localize around cellular inclusions and are surrounded by ferritin nanoparticles identified using EELS spot analysis

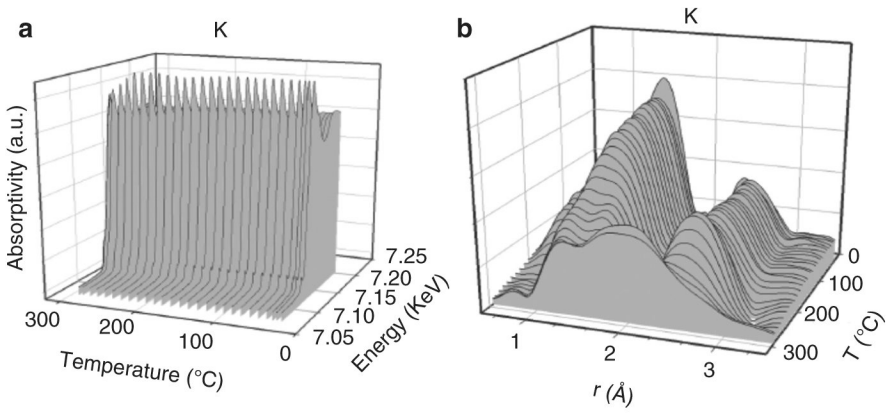

Fig. 4.16.

(**a**) XANES spectra for iron oxide; (**b**) EXAFS recorded during heating

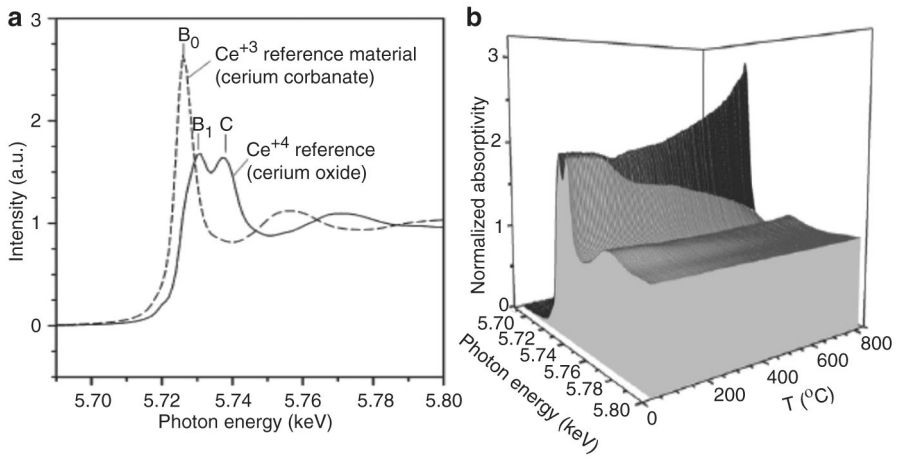

Fig. 4.17.

(**a**) XANES for Ce+3 and Ce+4 and (**b**) XANES as a function of heating